



# Evolutionary and pulsation properties of AGB stars

P.R. Wood

Research School of Astronomy and Astrophysics, Australian National University, Cotter Road, Weston Creek ACT 2611, Australia, e-mail: wood@mso.anu.edu.au,

**Abstract.** This paper discusses the evolution of AGB stars, the important question of mass loss, and variability in AGB stars.

**Key words.** Stars: mass loss – Stars: AGB and post-AGB – Stars: carbon – Stars: late-type – Stars: binaries – Stars – evolution

## 1. Introduction

The Asymptotic Giant Branch (AGB) is the phase of evolution in low and intermediate mass stars ( $M \lesssim 7 M_{\odot}$ ) following the completion of He burning in the central core. The position of AGB stars in the HR-diagram is shown in Fig. 1, relative to other evolutionary stages.

The spectra of AGB stars fall into very characteristic groups: the oxygen-rich stars, with spectra dominated by oxygen-containing molecules such as TiO, carbon-rich stars with spectra dominated by molecules containing carbon (e.g. CN,  $C_2$ ), and rarer stars in between with  $C/O \approx 1$  (S stars). Examples of these spectra are shown in Fig. 2. The existence of these stars indicates that the products of helium burning in the interior of the star are being brought to the stellar surface. Any theory of AGB evolution must be able to explain this.

While changes due to nuclear processes in the stellar interior occur on timescales of  $\sim 10^5$  years, the outer envelopes of AGB stars pulsate on timescales of  $\sim 10$ -1000 days. The pulsations are first seen with very small amplitude

and short period at low luminosities. The pulsations grow in amplitude with increasing luminosity up to amplitudes in bolometric magnitude of  $\sim 1$  mag. and periods typically of 500-1000 days. This large amplitude pulsation has a major consequence - it causes a very large increase in the mass loss rate, so that essentially all the envelope outside the nuclear burning core is lost. The star then evolves from the AGB through the post-AGB phase to the planetary nebula phase and ultimately to the white dwarf stage. During the planetary nebular phase, the envelope material lost in the AGB stellar wind is illuminated by energetic photons from the remnant star, thus creating the glowing planetary nebula.

In the remainder of this article, I will discuss the interior nuclear evolution of AGB stars, mass loss from them, and the variability observed on timescales of days to years.

## 2. The evolution of AGB stars

AGB stars have large, low density convective envelopes of radius several hundred  $R_{\odot}$  surrounding a dense, electron-degenerate core of carbon and oxygen. Between the envelope

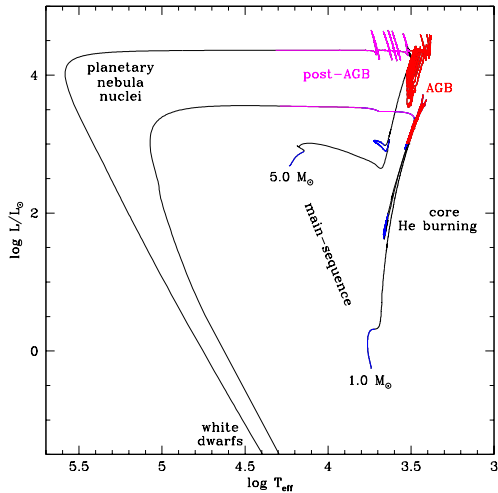


**Fig. 1.** Evolutionary tracks for stars of mass 1 and 5  $M_{\odot}$  and an initial solar-like composition of  $Y=0.25$  and  $Z=0.016$  (from Vassiliadis & Wood 1993). The AGB is the cool, luminous part of the tracks between the core helium burning clump (1  $M_{\odot}$ ) or loop (5  $M_{\odot}$ ) and the post-AGB phase, where the star evolves at nearly constant luminosity to the hot region occupied by planetary nebula nuclei. Helium shell flashes cause the star to move up and down the AGB multiple times, with excursions in  $T_{\text{eff}}$  being more prominent at 5  $M_{\odot}$  because of the large amount of mass lost during this phase of evolution.

and the core are hydrogen and helium burning shells, whose typical energy production can be seen as a function of time in Fig. 3. In the early AGB phase, following exhaustion of helium in the core, the H and He shells burn smoothly, but the He shell soon becomes unstable and starts a series of thermal relaxation cycles (Schwarzschild & Härm 1965). The He burning shell is effectively dormant for about 80% of the time, but at the end of each dormant period, it ignites furiously (but hydrostatically), reaching peak energy generation rates of  $\sim 10^8 L_{\odot}$  in the more massive cores. After several hundred years, the helium shell drops back to burning at a rate roughly in equilibrium with the surface luminosity of the star, taking over from the H burning shell as the main energy source. Over the next  $\sim 20\%$  of the shell flash cycle, the He burning shell burning rate gradually declines, while the H burning shell

rate increases to again become the dominant energy source, so that a new shell flash cycle begins.

The duration of a shell flash cycle, like most properties of the nuclear burning core, depends mostly on the core mass (e.g. Wood & Zarro 1981; Boothroyd & Sackmann 1988a). For a 1  $M_{\odot}$  AGB star with a typical core of mass  $\sim 0.6 M_{\odot}$  the cycle length is  $\sim 10^5$  years, while for an AGB star of initial mass more than  $\sim 5 M_{\odot}$  and a core mass of 0.9  $M_{\odot}$ , the cycle length is  $\sim 10^4$  years.

A very important aspect of AGB evolution is mass loss. The loss of essentially all the hydrogen-rich envelope is what terminates AGB evolution and leaves a compact remnant star that evolves through the parts of the HR diagram occupied by post-AGB stars, planetary nebular nuclei and white dwarfs (Fig. 1). Fig 3 shows the typical evolution of the mass loss rate and the mass in a 1  $M_{\odot}$  AGB star - many more examples are given in Vassiliadis & Wood (1993). It is particularly notable that mass tends to be ejected in multiple stages, which coincide with the brighter parts of the shell flash cycle when the H-burning shell is active. The mass loss process in AGB stars is discussed further in the next section of this paper.

The large energy release at a helium shell flash and its subsequent transport by convection leads to mixing processes that bring nuclear burning products, especially carbon and s-process elements, to the stellar surface: this process causes the transformation of AGB stars from oxygen-rich M stars to carbon stars with  $C/O > 1$ . The material ejected from AGB stars is a major source of enrichment of the interstellar medium in  $^{12}\text{C}$  and heavy s-process elements.

A general overview of the mixing processes is shown in Fig. 4. When the He shell ignites and releases a large amount of energy, the resulting temperature gradient is sufficient to drive convective energy transport, creating the Intershell Convective Zone. This zone carries the carbon produced by He burning outward, but not to the convective envelope, so that carbon is not directly mixed to the stellar surface. However, when the energy dumped into the He

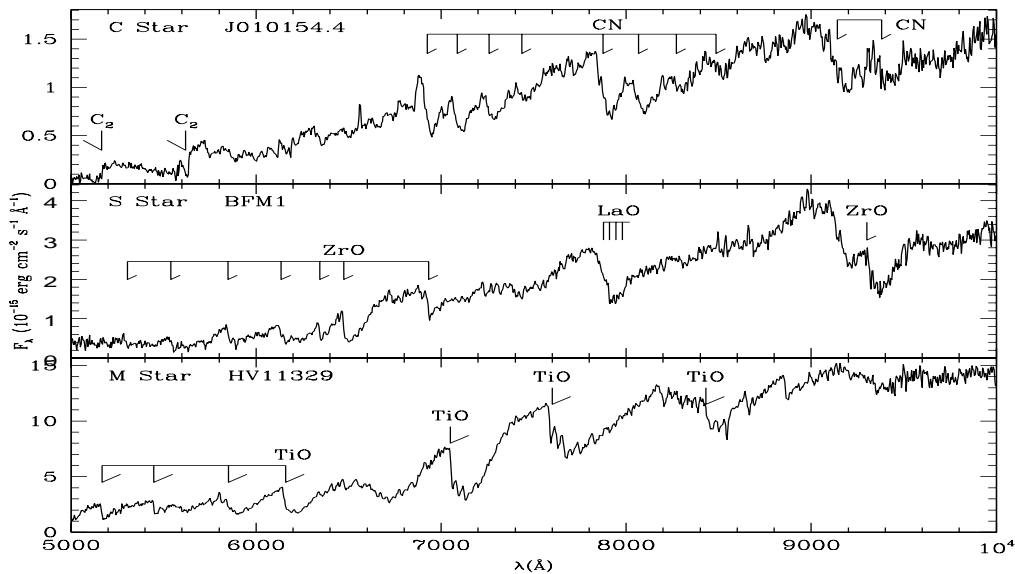


**Fig. 2.** The distinctive spectra of an M star, an S star and a C star. The sequence M→S→C corresponds to a change from  $C/O < 1$  to  $C/O \sim 1$  to  $C/O > 1$ . M stars have spectra dominated by molecules containing oxygen (e.g. TiO, VO) while C star spectra are dominated by molecules containing carbon (e.g. CN,  $C_2$ ). Some of the stronger bands are marked on the figure.

burning zone finally escapes from the core into the envelope, after the Intershell Convective Zone has disappeared, the envelope convection moves inward in mass and dredges up carbon-rich material within the mass region previously occupied by the Intershell Convective Zone. This process is called the Third Dredge-Up and is the mechanism by which carbon stars are formed.

Another important nuclear process that occurs in AGB stars is s-process nucleosynthesis, wherein heavy elements are created by the addition of neutrons to relatively abundant nuclei, such as those in the Fe-peak. For the process to occur, a source of neutrons is required. These neutrons come from two sources in AGB stars: the reactions  $^{12}\text{C}(p,\gamma)^{13}\text{N}(\beta^+\nu)^{13}\text{C}(\alpha,n)^{16}\text{O}$  and  $^{14}\text{N}(\alpha,\gamma)^{18}\text{F}(\beta^+\nu)^{18}\text{O}(\alpha,\gamma)^{22}\text{Ne}(\alpha,n)^{25}\text{Mg}$ . The first set of reactions need to occur in a region with a restricted number of protons, so that the  $^{13}\text{C}$  is not converted to  $^{14}\text{N}$  by proton absorption as would be the case with the CNO cycle operating in a H-rich region. Furthermore, the temperature needs to be higher than that in

the vicinity of the H-burning shell if the reaction  $^{13}\text{C}(\alpha,n)^{16}\text{O}$  is to occur. The first condition (low H abundance) occurs in the partial mixing region left at the bottom of the H-rich convective envelope by third dredge-up (the light grey region in Fig. 4). The details of the amount of mixing here are very uncertain, but some sort of semi-convection seems to be involved (Hollowell & Iben 1988). Because of the uncertainties in current evolution models, most nucleosynthesis calculations treat the amount of mixing (size of the “convective pocket”) as a free parameter. The second condition (sufficiently high temperatures) was found by Straniero et al. (1995) to exist in the convective pocket *between* He shell flashes. Although the reaction rates are slow, there is sufficient time for the s-process to occur in this interval. At the next He shell flash, s-process elements so produced are engulfed by the new intershell convection zone and then partially dredged-up to the stellar surface by the subsequent third dredge-up event. Other s-process elements remain in the convective pocket at the base of the third dredge-up zone, ready to

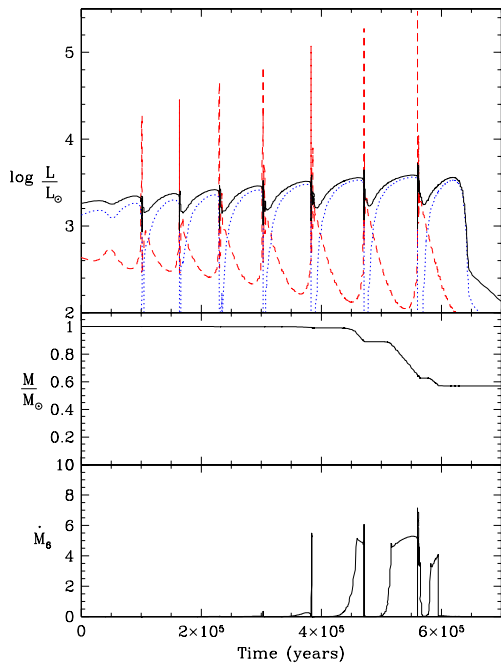


**Fig. 3.** The variation of  $L$ ,  $L_H$  (dotted line),  $L_{He}$  (dashed line),  $M$  and  $\dot{M}$  with time for a  $1 M_{\odot}$  AGB star. This solar metallicity model is from the calculations of Vassiliadis & Wood (1993).

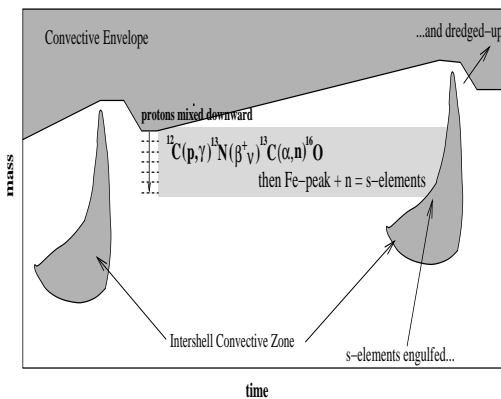


**Fig. 4.** A schematic diagram showing the positions of convection regions (dark grey) in the (mass fraction, time) plane. The light grey area is the region in which s-process nucleosynthesis occurs between He shell flashes. From Lattanzio & Wood (2004).

be further enhanced with neutrons in the next inter-flash interval.

The second set of neutron-producing reactions also contribute to s-process nucleosynthesis.  $^{14}\text{N}$  left over from the CNO cycle is readily burnt to  $^{22}\text{Ne}$  soon after He burning shell ignition. However, the final reaction  $^{22}\text{Ne}(\alpha, n)^{25}\text{Mg}$  requires temperatures near  $3 \times 10^8$  K, and is important mainly in the intershell convection zone of the more massive cores of the more massive AGB stars (e.g. Hollowell & Iben 1988).

Because the intershell convection zone contains material which is repeatedly exposed to a slow neutron flux, each time from freshly ingested source material, it is possible to build up *heavy* s-process elements. This is in contrast to the s-process that occurs in the cores of massive stars, when only a single exposure occurs and mainly light s-process elements are produced (Truran & Iben 1977). For a comprehensive examination of mixing processes and nucleosynthesis in AGB stars, see Lattanzio & Wood (2004).

A consistent problem with all studies of mixing in AGB stars is our lack of knowledge of convective processes, especially the amount of overshoot occurring at the edges of convective regions. Convection is usually treated by the mixing length theory, and it is well known that the adopted mixing length significantly affects the amount of dredge-up (Wood 1981; Boothroyd & Sackmann 1988b; Lattanzio 1989). Increasing the mixing-length enhances dredge-up. Attempts are now being made to study mixing in AGB stars by using multi-dimensional fluid dynamics (e.g. Herwig et al. 2006), rather than simple theories like the mixing-length theory. Much work remains to be done in this area.

The problems with numerical simulations of AGB stars has led to the creation of synthetic models of AGB evolution in which various aspects of the evolution, such as the amount of dredge-up at each helium shell flash and the minimum core mass at which dredge-up occurs, are treated as free parameters (see Marigo & Girardi (2007) and references therein for recent models). The parameters of these models are then calibrated against observational data, such as the luminosities of carbon stars in the LMC and SMC. The syn-

thetic model calculations are useful when wide areas of parameter space (initial  $M$  and abundance) are to be explored.

### 3. Mass loss from AGB stars

Mass loss dominates the late evolution of AGB stars, leading to loss of all but a tiny part of the H-rich envelope. At this stage, the star shrinks and evolves across the HR-diagram from  $T_{\text{eff}} \sim 3000$  K to  $T_{\text{eff}} \sim 10^5$  K. Mass loss from AGB stars seems to occur via two distinct mechanisms.

In AGB stars (and RGB stars on the first ascent of the giant branch) with no, or low amplitude, pulsation, the mass loss rates are quite low ( $\lesssim 10^{-7} M_{\odot}/\text{yr}$ ). The winds from these stars are thought to be driven by a chromosphere energized by deposition of magneto-acoustic energy generated in the convective envelope (e.g. Schröder & Cuntz 2005). In many AGB evolution calculations, this early mass loss is treated by the simple dimensional formula given by Reimers (1975):

$$\dot{M} = 4 \times 10^{-13} \eta LR/M,$$

with  $\dot{M}$  in  $M_{\odot} \text{ yr}^{-1}$  and  $L$ ,  $R$  and  $M$  in solar units. The constant  $\eta$  is usually adjusted so as to reproduce the mass loss observed to occur on the RGB in globular clusters, where  $0.2\text{--}0.3 M_{\odot}$  must be lost in order to reproduce the morphology of the Horizontal Branch. This normalization requires  $\eta \sim 0.5$  (Renzini & Fusi Pecci 1988).

Recently, Schröder & Cuntz (2005) have suggested a modification to Reimers' law to take into account estimates of the rate of magneto-acoustic heating of the chromosphere and the fact that the stellar wind starts from the top of the chromosphere rather than from the photosphere. Their formula, in a form close to that of Reimers' Law, is

$$\dot{M} = 8 \times 10^{-14} \eta' \frac{LR}{M} \left( \frac{T_{\text{eff}}}{4000\text{K}} \right)^{3.5} \left( 1 + \frac{g_{\odot}}{4300g_*} \right),$$

where  $g$  is the surface gravity and  $\dot{M}$  is in  $M_{\odot} \text{ yr}^{-1}$ . The constant  $\eta'$  is equal to unity according to Schröder & Cuntz (2005) if the

formula is to reproduce the observed globular cluster mass loss. The Schröder-Cuntz formula and the Reimers formulas generally give mass loss rates that agree to within a factor of 2 if  $\eta \sim 0.5$  and  $\eta' \sim 1.0$  (see Fig. 5). With the Schröder-Cuntz formula mass loss is more concentrated to the higher luminosities because of the gravity-dependent term.

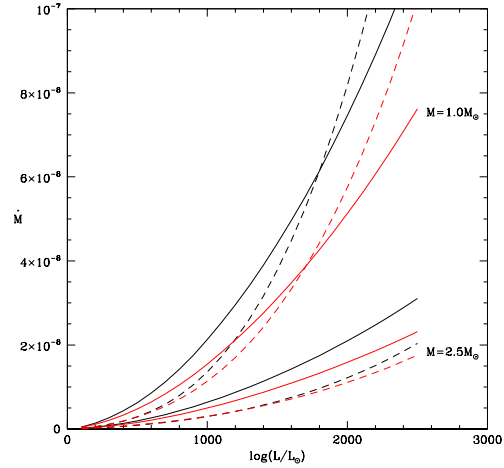


**Fig. 5.** The mass loss rate ( $M_{\odot}/\text{yr}$ ) plotted against  $\log(L/L_{\odot})$  for red giant stars of mass 1 and  $2.5 M_{\odot}$ , and abundances  $Z=0.02$  (thick lines) and  $Z=0.004$  (thin lines). Mass loss rates from Reimers' formula are shown as solid lines, while loss rates from the Schröder-Cuntz formula are shown as dashed lines.

Reimers-like mass loss rates are not sufficient to produce the mass loss rates of up to a few  $10^{-5} M_{\odot} \text{ yr}^{-1}$  that are observed in AGB stars (these are often called *superwinds*). The two defining characteristics of these high mass loss rate stars is that they are strong mid-IR emitters (because their winds are very dusty), and they are large amplitude pulsators. The dust is essential, since radiation pressure on the dust grains is the mechanism by which the wind is given the velocity (momentum) necessary to escape the star (e.g. Kwok 1975). In luminous AGB stars, the net acceleration of radiation pressure and gravity is outward once dust has formed in the circumstellar wind material.

The role of pulsation is to increase the density of gas and grains at the radius where grains form - it does not provide a significant amount of momentum to the wind. This can be seen in Fig. 6, which shows that pulsation can easily increase the density near the grain formation radius in a Mira variable by factors of  $\sim 100$ , while leaving the wind velocity almost unchanged. Since the mass loss rate  $\dot{M} = 4\pi R^2 \rho v$ , an increase in  $\rho$  by a factor of 100 while  $v$  remains unchanged at a given radius will increase  $\dot{M}$  by a factor of 100.

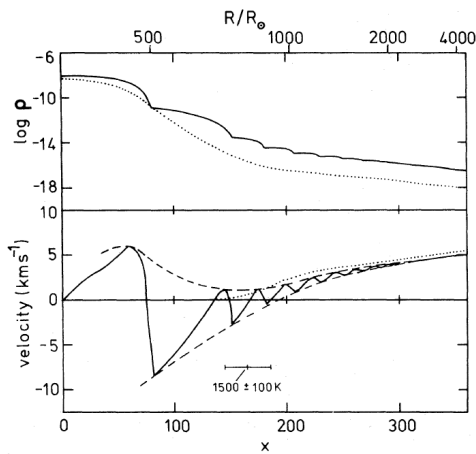


**Fig. 6.** A plot showing how pulsation in a Mira variable can increase the density in the vicinity of the sonic point by a factor of  $\sim 100$ . Solid lines show profiles of gas density ( $\rho$ ) and velocity in a pulsating model, while dotted lines show these quantities in a non-pulsating model. The quantity  $x$  is a radial coordinate. From Wood (1979).

Reliable modelling of the superwind mass loss in AGB stars requires a detailed knowledge of the grain formation process. For carbon stars, the physics of grain formation seems well established, and many models of winds in carbon stars have been made (e.g. Höfner & Dorfi 1997; Winters et al. 2000; Wachter et al. 2002; Woitke 2006a). However, the details of grain formation in oxygen rich stars is much more poorly known. Some recent wind models for oxygen rich stars have been attempted by Winters et al. (2000), Jeong et al.

(2003) and Woitke (2006b), but most such models seem to have problems starting the grain growth and getting grains with enough opacity for radiation pressure to create a wind. Höfner & Andersen (2007) have proposed a controversial solution to this problem involving a mixture of both carbon-rich and oxygen-rich grains.

If grain growth is assumed to have occurred, and an appropriate grain opacity is assumed, then mass loss rates can be derived as a function of stellar properties (e.g.  $M$ ,  $L$ , pulsation period). An extensive series of such models were made by Bowen (1988), although the input physics of the grains and post-shock cooling was very crude. More recent studies (e.g. Wachter et al. 2002) include more detailed physics of grain formation processes, and should begin to yield reliable mass loss rate estimates. Another factor that is starting to be studied in wind modelling is deviation from spherical symmetry (Woitke 2006a; Freytag & Höfner 2008).

In the absence of reliable models, it has been necessary to use empirical estimates of mass loss rates in stellar evolution calculations. Two widely used mass loss rate formulae are those of Vassiliadis & Wood (1993) and Bloeker (1995). Vassiliadis & Wood (1993) compiled mass loss rates derived from CO microwave observations of AGB winds and found that there was a good correlation of  $\dot{M}$  with pulsation period alone. The mass loss rate rose very rapidly with pulsation periods from 400–500 days, then flattened out for longer periods. Bloeker (1995) used the Bowen (1988) models and other observational considerations as a guide to produce a mass loss formula that is a power law in  $L$ ,  $R$  and  $M$ , as is the Reimers' formula.

The advent of the Spitzer space telescope has led to the possibility of measuring mass loss rates for AGB stars in the Magellanic Clouds. It turns out that, because of the sub-solar metallicity of the stars in the SMC and LMC, all evolved AGB stars with superwinds and initial masses less than  $\sim 3 M_\odot$  are carbon stars. Mass loss rates for a large number of these stars, all at the known distances of the LMC and SMC, have been derived

by Groenewegen et al. (2007). Using pulsation theory, it is possible to derive the current masses for these AGB stars. In Fig. 7, the mass loss rate for Magellanic Cloud carbon stars is shown as a function of pulsation period  $P$ , luminosity and current mass. Note that since the mass loss rates are derived from mid-IR observations of dust in the circumstellar envelopes of these stars, they are really scaled estimates of the dust mass loss rate. To convert the dust to the total (dust plus gas) mass loss rate, a gas/dust mass ratio is required: Groenewegen et al. (2007) assume a value of 200.

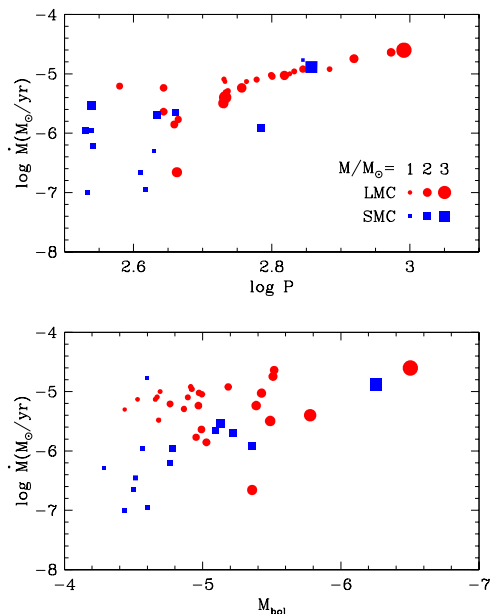


**Fig. 7.** The rate of mass loss from SMC and LMC AGB stars plotted against the log of the pulsation period  $P$ . The mass loss rates are based on dust-modelling of mid-IR spectra from the Spitzer Space Telescope (Groenewegen et al. 2007). The diameter of each symbol is proportional to the pulsation mass of the central star. The key shows the size of symbols for masses of 1, 2 and 3  $M_{\odot}$ . From Wood (2007).

For periods less than 500 days in Fig. 7, the mass loss rate varies enormously at a given pulsation period, and this variation does not

seem to obviously correlate with luminosity or mass. These stars appear to be at the stage of turning on their superwind mass loss (presumably because their pulsation amplitude is growing). They correspond to the stars which have very rapidly increasing mass loss rate for  $P < 500$  days in the mass loss formula of Vassiliadis & Wood (1993).

A remarkable feature of Fig. 7 is that stars with  $P > 500$  days follow a very tight relation between mass loss rate and pulsation period, regardless of luminosity, mass or metal abundance (SMC or LMC). This relation between  $\dot{M}$  and  $P$  for  $P > 500$  days will be a very useful one for modelling the evolution of lower mass AGB stars that turn into carbon stars, and it would replace the upper mass loss rate limit given in Vassiliadis & Wood (1993).

More massive ( $M \gtrsim 3 M_{\odot}$ ) AGB stars tend to remain oxygen-rich during their late evolutionary stages. A corresponding empirical mass loss rate formula derived from Magellanic Cloud stars of this type is given by van Loon et al. (2005). Ultimately, any mass loss formulae for studying the evolution of AGB stars must reproduce the relation between initial stellar mass and final stellar mass. A recent compilation of observational estimates of initial and final masses for AGB stars is given by Marigo & Girardi (2007), along with theoretical reproductions of the relation based on synthetic AGB calculations.

#### 4. Variable AGB stars

AGB stars show a very great range in the characteristics of their variability. Fig. 8 shows a selection of typical light curves for AGB stars.

<sup>1</sup> This paper utilizes public domain data originally obtained by the MACHO Project, whose work was performed under the joint auspices of the U.S. Department of Energy, National Nuclear Security Administration by the University of California, Lawrence Livermore National Laboratory under contract No. W-7405-Eng-48, the National Science Foundation through the Center for Particle Astrophysics of the University of California under cooperative agreement AST-8809616, and the Mount Stromlo and Siding Spring Observatory, part of the Australian National University.

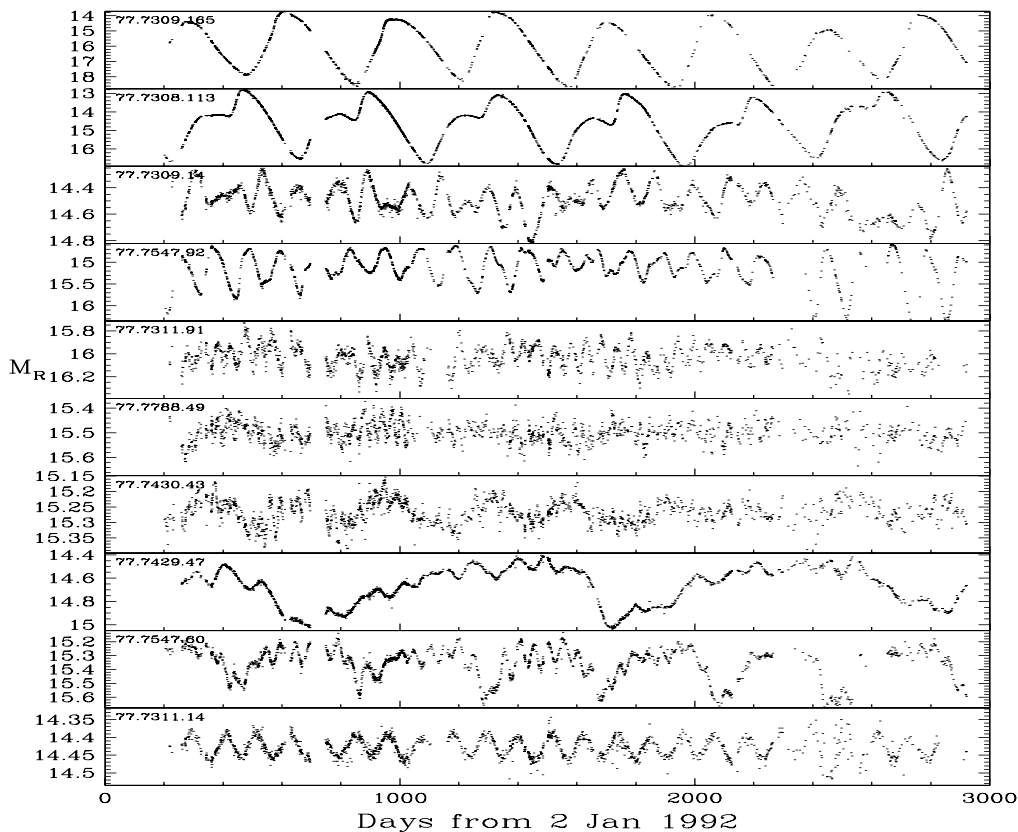


**Fig. 8.** MACHO<sup>1</sup> red light curves for a sample of red giant variables in the LMC.

Light curves of this quality have only become available as a result of surveys monitoring for microlensing events, the longest of which are MACHO, OGLE and EROS. These surveys cover the Magellanic Clouds, whose distances are known, so that period-luminosity (PL) diagrams can also be constructed for the variables. Before examining the light curves in Fig. 8, the PL diagram for variable red giants will be presented.

Fig. 9 shows the period-luminosity diagram for a large sample of red variable stars in the Large Magellanic Cloud. Similar plots can be found in many articles (e.g. Wood et al. 1999; Wood 2000; Ita et al. 2004; Soszyński et al. 2007; Fraser et al. 2005). There are clearly at least 6 sequences in Fig. 9. Different authors tend to use different labels for the various sequences - here the original la-

bellung of Wood et al. (1999) is used. However, since the original sequence B of Wood et al. (1999) was found to be two close sequences by Ita et al. (2004), their designation C' is used for the additional sequence. Also note that the position of sequence E is sometimes moved to the right by  $\log P = 0.301$  (a factor of 2) for reasons that are described below.

There is a significant increase in the number of stars on the sequences at luminosities below the luminosity of the red giant branch tip. Clearly, some RGB stars near the tip vary (Ita et al. 2002).

The light curves in Fig. 8 can now be discussed in relation to the PL sequences in Fig. 9. The top two light curves in Fig. 8 are typical of the light curves of Mira variables, the largest amplitude pulsating variable stars (the Miras are defined as having visible amplitudes



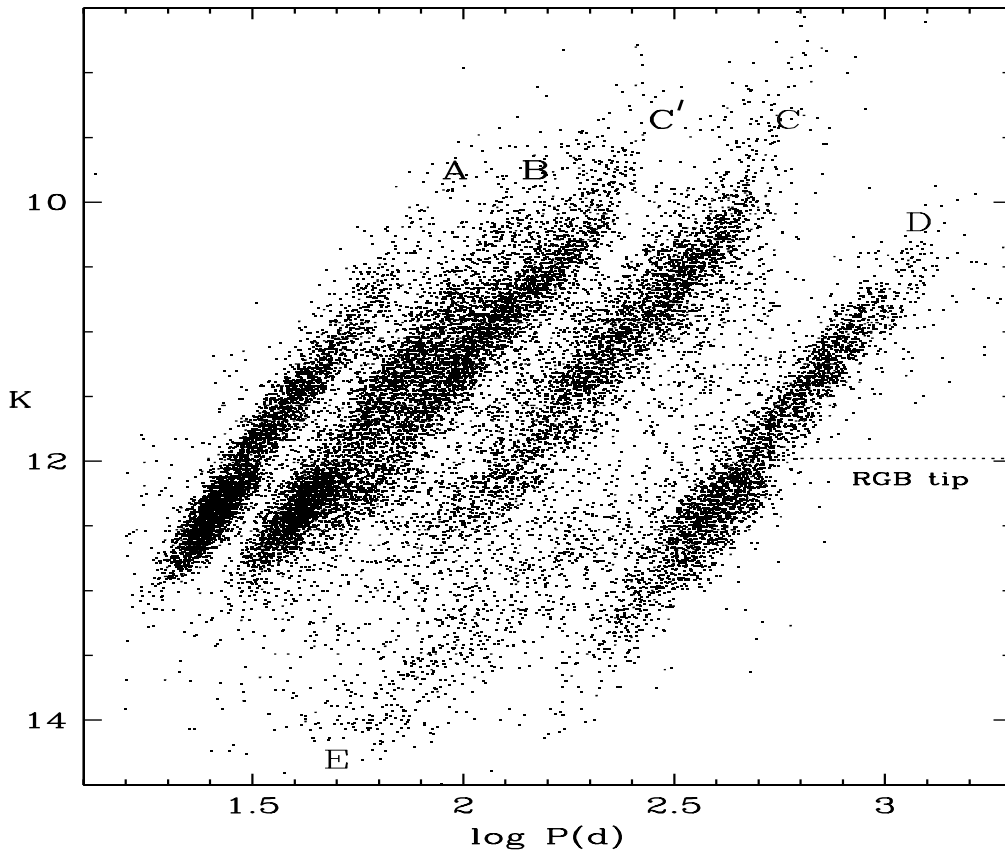


**Fig. 9.** The  $(K, \log P)$  diagram for red variable stars in the LMC.

greater than 2.5 mag. in the General Catalog of Variable Stars). These stars fall on sequence C, with a concentration to the higher luminosities. The double-humped light curves, like the second curve in Fig. 8, are common among the more luminous and massive stars. Analysis of periods and period ratios in these and other pulsating AGB variables (Wood et al. 1999) shows that the Miras are fundamental mode radial pulsators.

Moving down in Fig. 8, the next two light curves, with moderate amplitude, are typical of stars that would traditionally be described as Semi-Regular variables. They fall in the lower parts of sequence C and on sequence C', corresponding to fundamental and 1st overtone radial pulsation.

The next three light curves down the figure are even lower in amplitude and shorter in period. These stars mostly fall on the sequences-A and B, probably corresponding to pulsation in the second and third radial overtones. There is a hint of a faint sequence in Fig. 9 to short side of sequence A with some very small amplitude stars. This sequence is clearer in the analysis of OGLE red variables by Soszyński et al. (2004a). Soszyński et al. (2004a) claim that each of the sequences A and B is made up of several very closely spaced sequences. If that is the case, then the modes involved must be nonradial pulsation modes. However, there may be another explanation. It is well known that red giants tend to pulsate at a fixed frequency for approximately tens of cycles, then abruptly change period apparently

randomly by a few percent. This is best seen in O-C diagrams like those in Wood & Zarro (1981) and Wood et al. (2004). The reason for the sudden change in period is possibly due to a change in the number of convective cells in the convective envelope. The Fourier spectrum of an individual star's light curve in this case will be much broader than expected for a coherent oscillation for the full duration of the observation period, and it may show closely spaced peaks. Further analysis is required to see if the sequence A and B stars really do fall on discrete, closely spaced sequences.

The next two panels of Fig. 8 (2–3 from the bottom) show stars that have a short period, primary oscillation similar to that of the sequence A, B and C variables but also a long secondary period (LSP) of amplitude up to  $\sim 0.8$  mag. The origin of the LSP is unknown at the present time. Given that sequence C, about 4 times shorter in period, corresponds to radial fundamental mode pulsation, sequence D cannot correspond to a normal radial pulsation mode. These stars are discussed further below.

Finally, in the bottom panel of Fig. 8 there is a star with a relatively regular light curve. This is typical of one of the stars on sequence E, which extends well below the AGB and down the RGB. These stars are binaries showing ellipsoidal variations due to the fact that the red giant is distorted into an ellipsoidal shape by its unseen companion (Soszyński et al. 2004b). As the red giant completes one rotation in its orbit, the light curve goes through two cycles, since the flux received by the observer is mostly due to the change in the projected area of the red giant, and the projected area goes through two cycles per rotation due to the symmetry of the ellipsoidal shape. This is why the sequence E stars are sometimes plotted in the P-L diagram with twice the light curve period, since then  $P$  corresponds to the orbital period of the binary. A plot (Fig. 10) of the light and radial velocity curves of one of these stars demonstrates clearly the effect. The radial velocity of the red giant goes through one cycle as it makes one orbit in the binary system, while the light curve goes through two cycles.

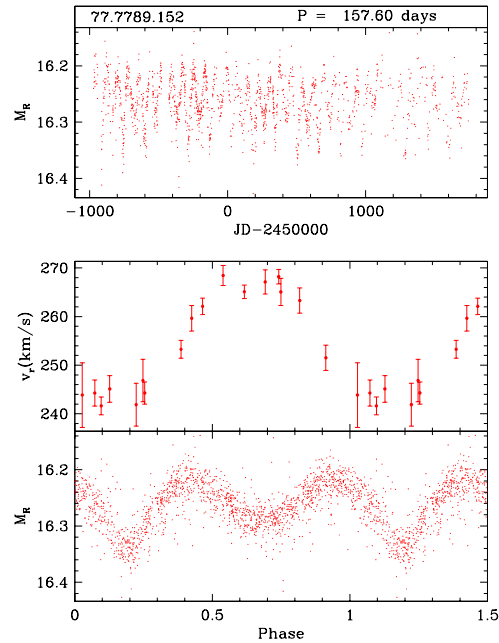


**Fig. 10.** Light and radial velocity curves for the sequence E variable MACHO 77.7789.152. In the top panel, the MACHO red magnitude is plotted against Julian date, while in the other two panels radial velocity and the MACHO red magnitude are plotted against phase of the 157.6 day cycle.

A subset consisting of about 10% of the sequence C stars show light curves that are far from sinusoidal, exhibiting sharp peaks during part of the variability cycle. An example is shown in Fig. 11. Modelling of the light curves of these stars by Soszyński et al. (2004b) showed that they were likely to be eccentric binaries. The velocity curve in Fig. 11 shows that this is indeed the case. These stars present a major problem, since tidal theory suggests that they should circularize their orbits on timescales of a few thousand years. Since they constitute  $\sim 0.3\%$  of luminous RGB stars which have a lifetime of  $\sim 10^8$  years, they seem to have lifetimes much longer than a few thousand years. Perhaps mass transfer at periastron in these systems can maintain the eccentricity (Soker 2000).

Given that the sequence E red giants are evolving to larger dimensions, they will

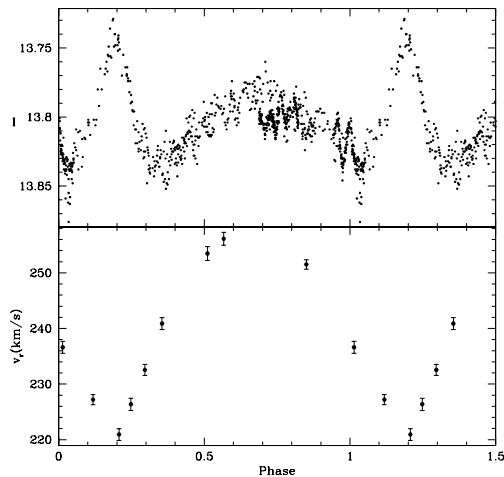


**Fig. 11.** Light and radial velocity curves for the sequence E variable OGLE052850.12-701211.2. In the top panel, the OGLE I magnitude is plotted against phase of the 662 day cycle, while in the lower panel radial velocity is plotted.

eventually fill their Roche lobes and lose their envelopes, presumably in a common envelope event (Hjellming & Webbink 1987). These stars may be the immediate precursors of bipolar planetary nebulae, binary post-AGB stars and RV Tauri stars, the latter two groups of stars consisting of binaries with periods and eccentricities similar to those of the sequence E stars (Van Winckel 2004).

The sequence D stars are the most puzzling of the red variables. When the sequence E stars are plotted in the PL diagram with  $P$  being the orbital period (see above), they fall on top of the sequence D stars (Soszyński et al. 2004b). Soszyński (2007) examined the light curves of many sequence D stars and he claimed that some of them had light curves that looked like ellipsoidal variables. Thus, there is a suggestion that the sequence D stars are binaries. Wood et al. (1999) originally suggested that the sequence D stars were close binaries, where the binary separation was a common multiple of the stellar radius, as for example in a Roche lobe filling red giant. In this case, the sequence of binaries would, from the laws of orbital motion, obey a relation  $P \sim r^3 M^{-1/2}$ , similar in form to the relation obeyed by the pulsating

variables on sequences A–C. Thus it would be expected that the binary and pulsation sequences would be parallel in the PL diagram, as observed.

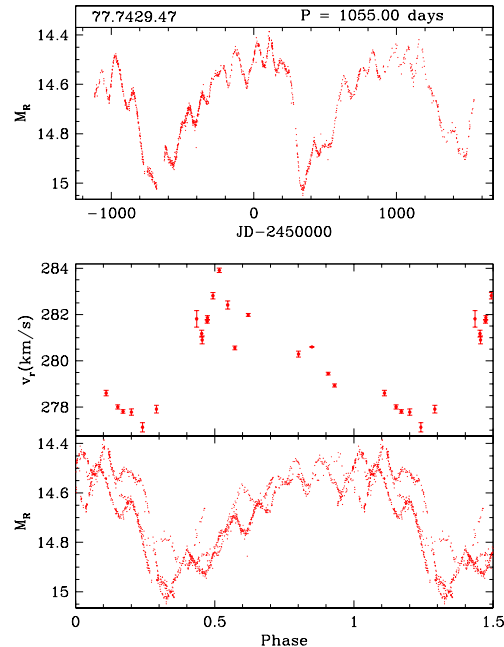


**Fig. 12.** Light and radial velocity curves for the sequence E variable MACHO 77.7429.47. In the top panel, the MACHO red magnitude is plotted against Julian date while in the other two panels radial velocity and the MACHO red magnitude are plotted against phase of the 1055 day cycle.

However, there are good reasons to think that the sequence D stars are not binaries (many of the following arguments, and others, can be found in Wood et al. 2004). Firstly, the light and velocity curves of sequence E ellipsoidal binary variables and sequence D stars are quite different. The light and velocity curves of a typical sequence D star is shown in Fig. 12. Comparing to Figures 10 and 11, it can be seen that the amplitude of the sequence D velocity curves ( $\sim 3.5 \text{ km s}^{-1}$ ) is an order of magnitude smaller than for typical sequence E star. Given the similar periods, this implies that all the companions of the sequence D binaries would have to have masses of  $\sim 0.05$ –

0.1  $M_{\odot}$ . Given that some 30–50% of luminous AGB stars show sequence D variability, the implication is that 30–50% of AGB stars have a close companion in the brown dwarf range. This is inconsistent with studies of nearby stars which show that very few stars have such companions - the so-called brown dwarf desert (Grether & Lineweaver 2006).

Another clear difference between the sequence D and sequence E light curves is that there is only one cycle of the light curve for each cycle of the velocity curve in sequence D stars, while the ellipsoidal sequence E variables show two cycles (the peaks being non-sinusoidal in the eccentric case). A particularly difficult problem for the binary model is that the velocity curves tend to have a similar shape, which is hard to explain in terms of orbital motion of binaries that should have random orientations on the sky.

If the sequence D stars are not binaries, then what are they? As discussed above, they cannot be normal-mode radial pulsators. Even if some sort of strange radial mode did exist, the observed change in radius obtained by integrating the radial velocity curve is not consistent with other estimated radius changes, such as estimated from the change in  $L$  and  $T_{\text{eff}}$  (Wood et al. 2004). An option considered by Wood et al. (2004) was a nonradial  $g$  mode of degree  $\ell \approx 2$  and low radial order. Such a mode has the correct period for an LSP. The main problem is that the amplitudes of such modes can be large only in radiative regions, and red giants are mostly convective with only a thin radiative layer on the outside. This is not likely to lead to  $g$ -mode oscillations with the observed radius amplitudes of  $\pm 10\%$ . On the other hand, one point in favour of a pulsation explanation is that the sequence D stars seem to occur at luminosities similar to those at which other modes become unstable (sequences A–C). Another feature of the sequence D stars noted by Wood et al. (2004) was the presence of an  $H\alpha$  absorption line, whose strength varied with the LSP. Since the stars in which these lines were observed had  $T_{\text{eff}} \sim 3000$  K, the presence of any  $H\alpha$  absorption line is an indication of a chromosphere. This chromosphere comes and goes with the LSP cycle. Perhaps

the LSP phenomenon is associated with magnetic fields in these stars. The sequence D mystery continues...

## References

- Blöcker T. 1995, *A&A* 297, 727  
 Boothroyd A.I., Sackmann I.-J. 1988a, *ApJ* 328, 653  
 Boothroyd A.I., Sackmann I.-J. 1988b, *ApJ* 328, 671  
 Bowen G.H. 1988, *ApJ* 329, 299  
 Fraser O.J., Hawley S.L., Cook K.H., Keller S.C. 2005, *AJ*, 129, 768  
 Freytag B., Höfner S. 2008, *A&A*, 483, 571  
 Grether D., Lineweaver C.H. 2006, *ApJ* 640, 1051  
 Groenewegen M.A.T., Wood P.R., Sloan G.C., Blommaert J.A.D.L., Cioni M.-R.L., Feast M.W., Hony S., Matsuura M., Menzies J.W., Olivier E.A., Vanhollebeke E., van Loon J. Th., Whitelock P.A., Zijlstra A.A., Habing H.J., Lagadec E. 2007, *MNRAS* 376, 313  
 Hjellming M.S., Webbink R.F. 1987, *ApJ* 318, 794  
 Herwig F., Freytag B., Hueckstaedt R.M., Timmes F.X. 2006, *ApJ* 642, 1057  
 Höfner S., Andersen A.C. 2007, *A&A* 465, 39L  
 Höfner S., Dorfi E. 1997, *A&A* 319, 648  
 Hollowell D., Iben I. Jr. 1988, *ApJL* 333, L25  
 Ita Y., Tanabé T., Matsunaga N., Nakajima Y., Nagashima C., Nagayama T., Kato D., Kurita M., Nagata T., Sato S., Tamura M., Nakaya H., Nakada Y. 2002, *MNRAS* 337, L31  
 Ita Y., Tanabé T., Matsunaga N., Nakajima Y., Nagashima C., Nagayama T., Kato D., Kurita M., Nagata T., Sato S., Tamura M., Nakaya H., Nakada Y. 2004, *MNRAS*, 347, 720  
 Jeong K.S., Winters J.M., Le Bertre T., Sedlmayr E. 2003, *A&A* 407, 191  
 Kwok S. 1975, *ApJ*, 198, 583  
 Lattanzio J.C. 1989, *ApJ* 344, L25  
 Lattanzio J.C., Wood P.R. 2004, in *Asymptotic Giant Branch stars*, eds. H.J. Habing & H. Olofsson, *Astron. and Ap. Library* (Springer), p.23.  
 Marigo P., Girardi L. 2007, *A&A* 469, 239

- Pignatari M., Gallino R., Käppeler F. Wiescher M. 2005, Nucl.Phys.A 758, 541
- Renzini A., Fusi Pecci F. 1988, ARA&A 26, 199
- Reimers D. 1975, in *Problems in Stellar Atmospheres and Envelopes*, eds. B. Bascheck, W.H. Kegel and G. Traving (Springer: Berlin), p.229
- Schröder K.-P., Cuntz M. 2005, ApJL 630, L73
- Schwarzschild M., Härm R. 1965, ApJ 142, 855
- Soker N. 2000, A&A, 357, 557
- Soszyński I. 2007, ApJ 660, 1486
- Soszyński I., Udalski A., Kubiak M., Szymański M., Pietrzyński G., Zebruń K., Szewczyk O., Wyrzykowski L. 2004a, Acta Astr., 54, 129
- Soszyński I., Udalski A., Kubiak M., Szymański M., Pietrzyński G., Zebruń K., Szewczyk O., Wyrzykowski L., Dziembowski W.A. 2004b, Acta Astr., 54, 347
- Soszyński I., Udalski A., Kubiak M., Szymański M., Pietrzyński G., Zebruń K., Szewczyk O., Wyrzykowski L., Ulaczyk K. 2005, Acta Astr., 55, 331
- Soszyński I., Dziembowski W.A., Udalski A., Kubiak M., Szymański M., Pietrzyński G., Wyrzykowski L., Szewczyk O., Ulaczyk K. 2005, Acta Astr., 57, 201
- Straniero O., Gallino R., Busso M., Chieffi A., Raiteri C.M., Limongi M., Salaris M. 1995, ApJ 440, L85
- Truran J.W., Iben I.Jr. 1977, ApJ 216, 797
- van Loon J.Th., Cioni M.-R.L., Zijlstra A.A., Loup C. 2005, A&A 438, 273
- Van Winckel H. 2004, MmSAI 75, 766
- Vassiliadis E., Wood P.R. 1993, ApJ 413, 641
- Wachter A., Schröder K.-P., Winters J.M., Arndt T.U., Sedlmayr E. 2002, A&A 384, 452
- Winters J.M., Le Bertre T., Jeong K.S., Helling Ch., Sedlmayr E. 2000, A&A 361, 641
- Woitke, P. 2006a, A&A 452, 537
- Woitke, P. 2006b, A&A 460, L9
- Wood P.R. 1979, ApJ 227, 220
- Wood, P. R. 1981, in *Physical Processes in Red Giants*, ed. I. Iben & A. Renzini, (Dordrecht: Reidel), 135
- Wood P.R. 2000, PASA 17, 18
- Wood P.R. 2007, ASPC 374, 47
- Wood P.R., Zarro D.M. 1981, ApJ 247, 247
- Wood P.R. and the MACHO Collaboration 1999, in IAU Symp. 191, *AGB Stars*, p. 151
- Wood P.R., Olivier E.A., Kawaler S.D. 2004, ApJ 604, 800